Characterization of Hydroxyapatite Derived from Scallop Shell Waste Synthesized by Sonochemical Method with Different Temperature Calcination

Diki Dwi Pramono[1], Poppy Puspitasari[1,2*], Aminnudin Aminnudin[1], Jeefferie Abd Razak[3]

[1]*Department of Mechanical and Industrial Engineering, Faculty of Engineering, Universitas Negeri Malang, Malang, Indonesia, 65145*
[2]*Centre of Advanced Materials for Renewable Energy, Universitas Negeri Malang, Malang, Indonesia, 65145*
[3]*Fakulti Teknologi dan Kejuruteraan Industri dan Pembuatan, Universiti Teknikal Malaysia Melaka, Melaka, Malaysia*
**Corresponding author: poppy@um.ac.id*

Article history:
Received: 13 June 2024 / Received in revised form: 19 July 2024 / Accepted: 26 July 2024
Available online 6 November 2024

ABSTRACT

One common bio-ceramic material used in the biomedical industry is hydroxyapatite. Because of its crystallographic and molecular resemblance to the hard tissues of the human body, hydroxyapatite is thought to form. Scallop shells are one natural source of hydroxyapatite, which is high in calcium. This study examines how the calcination temperature affects the characteristics of hydroxyapatite made from leftover scallop shell. Hydroxyapatite was synthesized via the sonochemical method, with calcination conducted at temperatures of 900°C, 1000°C, and 1100°C. The hydroxyapatite that was prepared was assessed using X-ray diffraction (XRD) to determine the phase and crystallite size, Scanning Electron Microscopy (SEM) to conduct a morphological investigation, and Fourier Transform Infrared (FTIR) spectroscopy to conduct a functional group analysis. Phases resulting from varying calcination temperatures include hydroxyapatite and β-tricalcium phosphate. The crystallite size of hydroxyapatite enhanced with rising temperature. The morphology of hydroxyapatite exhibited agglomeration in all samples, with grain size escalating alongside the increase in calcination temperature. The functional groups generated under the three temperature fluctuations include O-H, P-O, PO_4^{3-}, and O–P–O groups. The calcination temperature significantly influences the characteristics of produced hydroxyapatite and impacts its biocompatibility as a bone implant material.

Keywords: *Calcination, hydroxyapatite, scallop shell, sonochemical, temperature*

I. Introduction

Hydroxyapatite (HAp) is another form of calcium phosphate extensively utilized in the biomedical sector due to its biocompatibility, bioactivity, and non-toxicity [1]. Hydroxyapatite can be derived from natural sources rich in calcium, including clam shells, eggshells, coral, and animal bones [2]-[4]. The scallop shell is a natural substance rich in calcium. The scallop shell (*Amusium pleuronectes*) has calcium mostly as calcium carbonate (CaCO3), constituting 97-99% of its composition. In 2018, the production of scallop shells in the Surabaya area amounted to 412.2 tons [5], [6]. Currently, research related to scallop shells is widely used as a biodiesel catalyst, used to make filler as a base material for making composite boards, and used to make chitosan as a wastewater coagulant [7]-[10]. The high calcium content and the high availability provide a potential opportunity for scallop shell waste to be used as a HAp base material [11].

DOI: 10.17977/um016v8i22024p400

Chemical synthesis methods include hydrothermal, co-precipitation, sol-gel, hydrolysis, emulsion, and sonochemical processes may be used to get HAp from natural sources [12]. Among the several synthetic approaches, the sonochemical technique is a practical and efficient way to synthesize HAp, nevertheless, it also yields HAp with very high purity [13]-[15]. This method is widely used to synthesize HAp because of its advantages: small particle size, good uniformity, and a large percentage of crystallinity [16]. However, HAp particles prepared by the sonochemical method can cause crystal structure degradation (lattice defects) due to excessive energy. This may be mitigated by using suitable calcination temperatures to efficiently eliminate lattice flaws while preventing excessive grain development or material degradation, which may result in the emergence of additional defects [17].

Calcination temperature is a critical factor in removing crystal lattice defects in HAp. Optimal calcination temperatures are necessary to eliminate lattice defects effectively without causing excessive grain growth or material degradation, which could introduce new defects [17]. Lower temperatures may not be sufficient for defect removal, while higher temperatures can lead to undesired outcomes [1]. Increasing the calcination temperature can lead to the crystalline growth of HAp particles, resulting in changes in particle morphology and a reduction in pore sizes and density. These alterations can reduce the contact surface between adsorbed ions and HAp, impacting the material's properties [18]. Moreover, high calcination temperatures can prompt the release of hydroxyl groups from HAp, generating new vacancies and defect sites in the material [19]. Hammood et al. [20] utilized bovine femur bone to generate natural hydroxyapatite (HAp), revealing that the best calcination temperature for achieving near-pure HAp is 900°C. Agbabiaka et al. [21] shown that hydroxyapatite (HAp) calcined at 1000°C exhibits a stoichiometric ratio Ca/P = 1.65 comparable to that of real bone and possesses the propensity to agglomerate, hence forming holes essential for the circulation of bodily fluids. Therefore the selection of an appropriate calcination temperature is crucial in the production of HAp to ensure that the desired properties of the material, such as mechanical strength, porosity, and biocompatibility, can be achieved.

In this study, the effect of calcination temperature on HAp synthesised from scallop shell waste using sonochemical method was analysed. The temperatures used in this study are 900°C, 1000°C and 1100°C.

II. Material and Methods

1. Materials

This research used scallop shell waste collected from Pantai Kenjeran, Surabaya. Acetone (purity > 99.5%), diammonium hydrogen phosphate ((NH4)2.HPO4) (purity ≥ 99%), and Whatman filter paper (No. 41) were acquired from Sigma-Aldrich, USA. Deionized water of analytical quality was acquired from Onelab, Indonesia.

2. Preparation of Scallop Shell Waste

The pre-ground scallop shell was divided into two sections of 300 g each and placed in a vial ball mill. Next, 75 mL of acetone was poured into the planetary ball mill (MTI MSK-SFM-1, Korea). The milling operation was carried out for a duration of 5 hours, maintaining a rotational speed of 400 RPM. In order to transform the $CaCO_3$ powder into CaO powder, the milled samples were subjected to further calcination at 1100°C for 60 minutes in a muffle

furnace (MTI KSL-1750X, USA), as shown in reaction 1. The samples were then crushed to prevent aggregation.

$$CaCO_3 \rightarrow CaO + CO_2 \quad \text{..... (1)}$$
$$2CaO + 2H_2O \rightarrow 2Ca(OH)_2 \quad \text{..... (2)}$$

The produced CaO is then transformed into $Ca(OH)_2$ by exposure to air (water vapor) at ambient temperature for one day, as shown in reactions of Eq. (1) and Eq. (2).

3. Synthesis of Hydroxyapatite

Hydroxyapatite was synthesized through the incremental addition of 0.3M $(NH_4)_2.HPO_4$ to $Ca(OH)_2$ powder obtained from scallop shells, kept at a temperature of 40 ± 2°C for one hour, with agitation facilitated by a hotplate magnetic stirrer (Thermo Fisher Scientific, USA), as illustrated in the reaction of Eq. (3). The resulting suspension was sonicated for 90 minutes using an ultrasonic cell disruptor (Biobase UCD-2000, China). The sonicated suspension was left at room temperature for 24 hours. Afterward, it was centrifuged (Oregon LC-04R, China) at 3000 rpm for 15 minutes. The sediment obtained was subjected to decantation and subsequently rinsed with deionized water. The filtration process employed a Whatman paper filter. Ultimately, the filtered sediment underwent a drying process at 100°C for three hours. The sediment underwent grinding in a mortar and was then calcined in a muffle furnace at temperatures of 900°C, 1000°C, and 1100°C for 2 hours. Subsequently, the HAp samples were allowed to cool to ambient temperature prior to being subjected to crushing for one hour.

$$10Ca(OH)_2 + 6(NH_4)_2.HPO_4 \rightarrow Ca_{10}(PO_4)_6(OH)_2 + 6H_2O + 12NH_4OH \quad \text{... (3)}$$

4. Phase and Crystallite Size

Phase and crystallite size of HAp derived from scallop shell waste was characterized using XRD PANalytical X'Pert Pro (Malvern Panalytical, UK). The diffraction angle used for the scanning ranged between 10^o and 55^o. The phase of the HAp was analysed using Match! software, The Scherrer equation, which is stated in Eq. (4), was used in order to ascertain the size of the crystallites [22].

$$d = \frac{k\lambda}{\beta \cos\theta} \quad \text{..... (4)}$$

With the representation of d reflecting the size of the crystallite, the representation β denoting the full-width at half maximum (FWHM), the representation k being the constant (0.9), and the representation of λ being the wavelength (1.5406 Å).

5. Morphology

Morphological characterization was performed using the SEM Inspect-S50 type (FEI, Japan). The magnification is 50000× and 100000×. The HAp surface was covered with a layer of gold to increase the sample'sconductivity prior to observation.

6. Functional Groups

The functional groups were analyzed using the FTIR model Prestige 21 (Shimadzu Instrument, Japan) within the wavelength range of 4000-400 cm^{-1}.

III. Results and Discussions

1. Phase and Crystallite Size of Hydroxyapatite

Phase identification involved analyzing the crystal phases present in the HAp powder derived from scallop shell using X-ray diffraction techniques. The study also encompassed the analysis of crystallite sizes, crystal orientation, crystal imperfections, and phase composition in each phase.

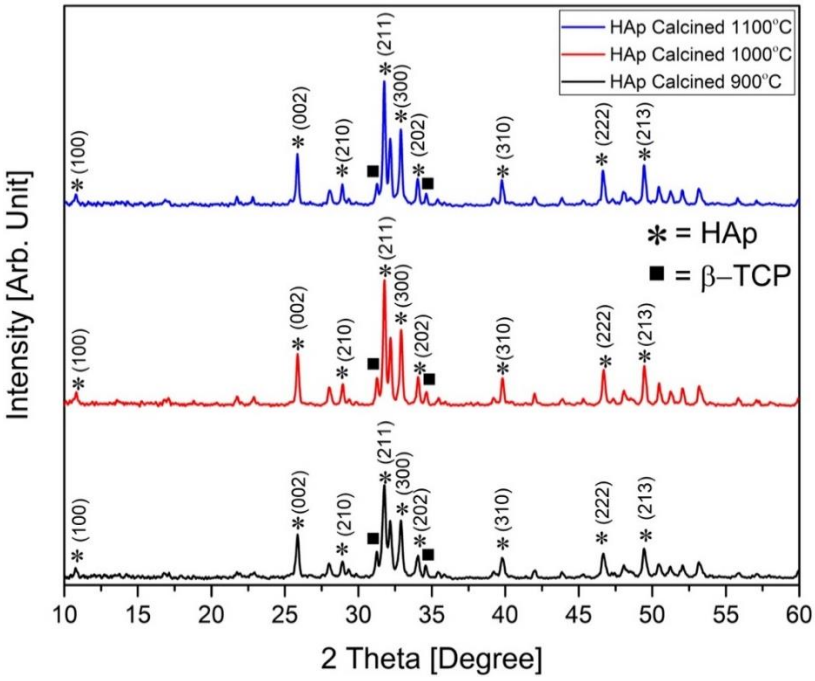

Fig. 1. XRD patterns of HAp derived from scallop shell waste

Table 1. Crystallite size of hydroxyapatite derived from scallop shell waste

Sample	FWHM [2theta]	Intensity [cts]	d-spacing [Å]	Bragg's Angle [2th]	Crystallite Size [nm]
HAp Calcined 900°C	0.2592	262.17	2.8157	31.8093	31.89
HAp Calcined 1000°C	0.2054	366.35	2.8158	31.7897	40.25
HAp Calcined 1100°C	0.2023	368.05	2.8179	31.7699	40.85

The diffraction pattern of the HAp sample derived from scallop shell waste is depicted in Figure 1. The result of XRD displays distinct diffraction peaks in the 2theta angle range corresponding to the crystal planes denoted by the Miller indexes, which are (100), (002), (210), (211), (300), (202), (310), (222), and (213). The sharp peaks observed were consistent regarding ICDD No. 01-079-8093, validating the successful synthesis of the HAp phase, which is defined by its hexagonal crystal structure [23], [24]. Additionally, the β-tricalcium phosphate (β-TCP) phase was identified in the sample with ICDD No. 04-014-2292 [25]. This appearance of β-TCP is attributed to the high calcination temperatures. High calcination temperatures can promote the release of hydroxyl groups from HAp resulting in new phases [19]. In a previous study conducted by Khiri et al. [26], it was observed that the production of the β-TCP phase occurred when the temperature at which calcination occurred raised from 1100°C to 1400°C. Other studies by Lee et al. [27] show that the formation of β-TCP

phase occurs at a starting temperature of 1000°C. In addition to the calcination temperature, the transformation of HAp to β-TCP can also be caused by the pH of the solution and the ultrasonic effect of the synthesis process [28].

Table 1 presents the crystallite size determined by the Scherrer equation. Based on this table, it shows that HAp calcined at 900°C, 1000°C, and 1100°C has an increase in peak intensity and crystallite size. The calcination process involves heat treatment of the sample to improve its purity. The calcination process results in thermal decomposition and the release of carbon dioxide, in addition, the application of heat causes the crystals within the grains to enlarge or grow [29], [30]. This phenomenon reappears with a rise in calcination temperature. The rate of crystal growth rises with a rise in the temperature of the calcination process, likely attributed to the presence of diffusing atoms [31].

2. Morphology of Hydroxyapatite

Morphological identification of HAp samples derived from scallop shell waste was carried out using SEM with a magnification of 50000× and 100000×.

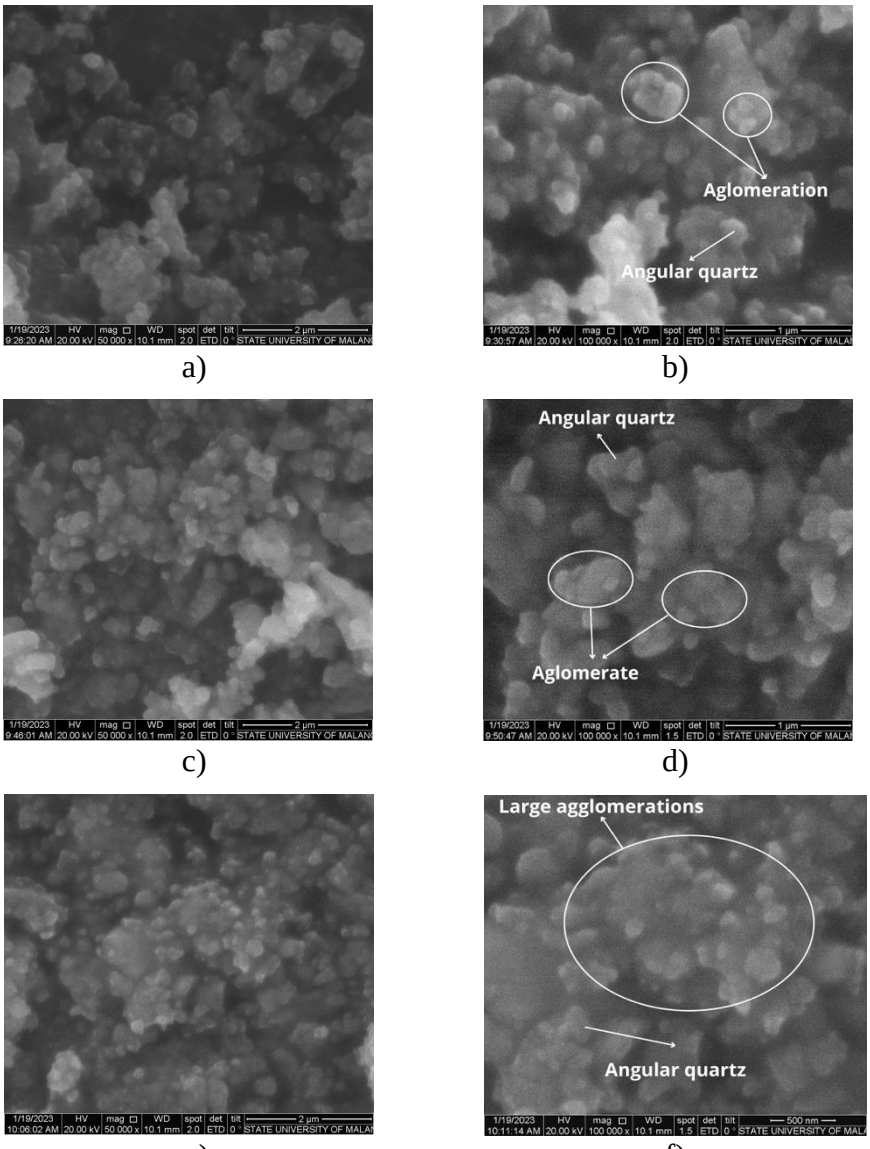

Fig. 2. SEM result of hydroxyapatite samples calcined a-b) 900^{o}C, c-d) 1000^{o}C and e-f) 1100^{o}C

Based on Figure 2, it shows that the HAp sample has an angular quartz particle shape with the agglomeration level of the sample increasing as the calcination temperature of the sample increases [32]. The calcination process, characterized by elevated thermal energy, significantly influences the physical characteristics, resulting in phase and structural transformations in the particles, which subsequently coalesce, leading to an increase in density (agglomeration) [33].

In the course of the observation, the sample subjected to a calcination temperature of 900°C exhibited a smaller grain size. Furthermore, there is a tendency for the grain size to increase throughout the calcination process. Applying heat leads to the enlargement or growth of the crystals within a grain [5], [34]. With an increase in the prescribed calcination temperature, this effect will continue to increase. As the size of the crystals in the grain increases, it causes each grain also to experience growth, resulting in a closer proximity of the grains [35], [36].

3. Functional Groups of Hydroxyapatite

Identification of functional groups of HAp samples derived from scallop shell using FTIR at wavelength 4000-400 cm^{-1}.

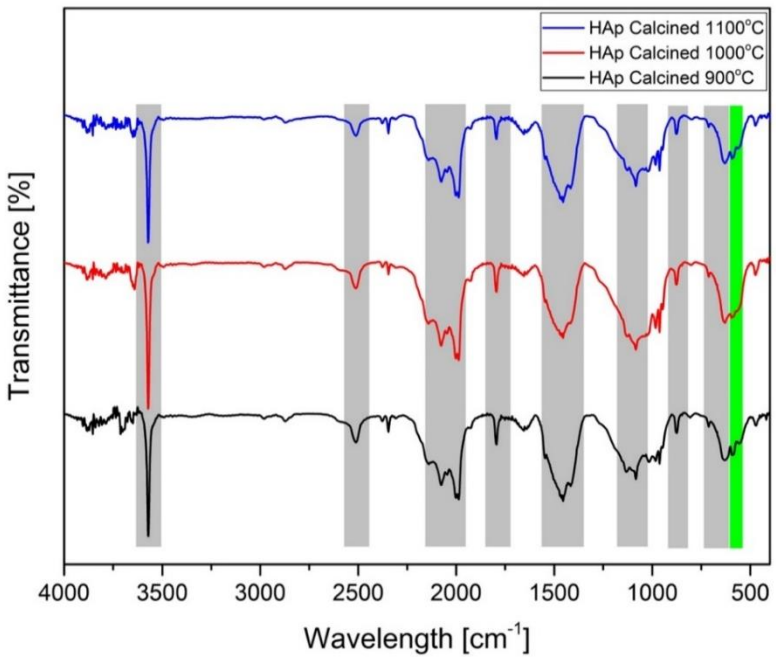

Fig. 3. Spectrum FTIR of hydroxyapatite derived from scallop shell waste

Table 2. FTIR peak description of hydroxyapatite derived from clamshell waste

Wavelength [cm^{-1}]	Descriptions
3567.59 and 646.15	Vibration of O-H bond
2509.88 and 1793.67	Stretching and bending of the hydrogen bond of the H_2O
1986.68 – 2140.99	Stretching P-O bonds
1549.41–1452.57 and 875.68	Carbonate groups
947.05–1168.86	Antisymmetric vibration of the PO_4^{3-} ion
617.22 and 646.15	O–P–O bending vibration of the PO_4 group in phosphate
590.23 and 552.57	Characteristic of the β-TCP phase

Based on Figure 3 and Table 2, shows that in all HAp samples, there is a peak at wavelength 3567.59 cm^{-1} which indicates vibration of O-H bond corresponding to the hydroxyl group of the HAp phase [37], [38]. The peaks observed at wavelengths 2509.88 cm^{-1} and 1793.67 cm^{-1} are indicative of the stretching and bending motions associated with the hydrogen bond in H_2O [39]-[42]. The peak at 1986.68 – 2140.99 cm^{-1} is a bond from stretching P-O bonds from phosphate groups [43]. At wavelengths of 1549.41–1452.57 and 875.68 cm^{-1}, carbonate groups are produced, which are combined in the HAp structure [1], [38], while at wavelengths of 947.05–1168.86 cm^{-1}, the antisymmetric vibration of the PO_4^{3-} ion [20], [44]. Two peaks at wavelengths 617.22 and 646.15 cm^{-1} represent the O–P–O bending vibration of the PO_4 group in phosphate [45], [46]. Two small peaks (marked in green) at wavelengths 590.23 cm^{-1} and 552.57 cm^{-1} are indicative of the β-TCP phase [47].

IV. Conclusions

HAp was synthesized using the sonochemical method from clamshell waste at calcination temperatures of 900°C, 1000°C, and 1100°C. The resulting HAp was then analyzed for its phase, crystallite size, morphology, and functional groups. The treatment of HAp at various calcination temperatures resulted in the formation of HAp and β-tricalcium phosphate phases. Notably, the HAp sample subjected to a calcination temperature of 900 °C exhibited the smallest crystallite size. The morphology of HAp exhibits agglomeration within the sample, alongside a rise in particle size distribution as the calcination temperature escalates. The calcination treatments of HAp resulted in the formation of O-H, P-O, PO_4^{3-}, and O-P-O functional groups. Consequently, the calcination temperature significantly influences the characteristics of the synthesized HAp and impacts its biocompatibility as a material for bone implants.

Acknowledgment

The authors wish to acknowledge Universitas Negeri Malang for the opportunity, support, and guidance provided throughout the study of this paper.

References

[1] A.S. Hammood, S.S. Hassan, M.T. Alkhafagy, and H.L. Jaber, “Effect of calcination temperature on characterization of natural hydroxyapatite prepared from carp fish bones,” *SN Applied Science*, vol. 1, no. 436, pp. 1–12, 2019.

[2] M. Akram, R. Ahmed, I. Shakir, W.A. W. Ibrahim, and R. Hussain, “Extracting hydroxyapatite and its precursors from natural resources,” *Journal of Materials Science*, vol. 49, no. 4, pp. 1461–1475, 2014.

[3] P. Puspitasari, V. Yuwanda, Sukarni, and J.W. Dika, “The properties of eggshell powders with the variation of sintering duration,” in *IOP Conference Series: Materials Science and Engineering*, Institute of Physics Publishing, 2019.

[4] P. Puspitasari, M. Chairil, S. Sukarni, and N.S.W. Supriyanto, “Physical properties and compressibility of quail eggshell nanopowder with heat treatment temperature variations,” *Materials Research Express*, vol. 8, no. 5, pp. 1–7, 2021.

[5] P. Puspitasari and D.D. Pramono, “Phase identification, morphology, and compressibility of scallop shell powder (Amusium pleuronectes) for bone implant materials,” in *Nanotechnologies in Green Chemistry and Environmental Sustainability*, Boca Raton: CRC Press, 2022, pp. 5–25.

[6] Dinas Ketahan Pangan Dan Pertanian Kota Surabaya, “Produksi ikan laut menurut jenis nya (ton) 2013-2018,” Surabaya, Apr. 2020. Accessed: Jul. 23, 2024. [Online].

Available: https://surabayakota.bps.go.id/statictable/2020/04/29/664/produksi-ikan-laut-menurut-jenis-nya-ton-2013-2018.html
[7] A. Buasri, P. Worawanitchaphong, S. Trongyong, and V. Loryuenyong, "Utilization of scallop waste shell for biodiesel production from palm oil – optimization using Taguchi method," *APCBEE Procedia*, vol. 8, no. Caas 2013, pp. 216–221, 2014.
[8] A. Mufidun and A. Abtokhi, "Pemanfaatan filler serbuk cangkang kerang simping (Placuna placenta) dan matriks poliester sebagai bahan dasar pembuatan papan komposit," *Journal Neutrino*, vol. 9, no. 1, pp. 1–7, 2016.
[9] A. Pradifan, E. Sutrisno, and M. Hadiwidodo, "Studi penggunaan kitosan dari limbah cangkang kerang simping (Amusium Pleuronectes) sebagai biokoagulan untuk menurunkan kadar COD Dan TSS," *Journal Teknik Lingkungan*, vol. 5, no. 3, 2016.
[10] P. Puspitasari, D. D. Pramono, D. N. Fiansyah, A. A. Permanasari, N. Mufti, and J. A. Razak, "Biodiesel production from waste cooking oil using calcium oxide derived from scallop shell waste," *Clean Energy*, vol. 8, no. 2, pp. 113–126, Apr. 2024.
[11] F.Y. Syafaat and Y. Yusuf, "Influence of ca/p concentration on hydroxyapatite (Hap) from asian moon scallop shell (amusium pleuronectes)," *International Journal of Nanoelectronics and Materials*, vol. 12, no. 3, pp. 357–362, 2019.
[12] P. Arokiasamy, M.M.A.B. Abdullah, S.Z.A. Rahim, S. Luhar, A.V. Sandu, N.H. Jamil et al., "Synthesis methods of hydroxyapatite from natural sources: A review," *Ceramics International*, vol. 48, no. 11, pp. 14959–14979, 2022.
[13] S. Santhosh and S. Balasivanandha Prabu, "Thermal stability of nano hydroxyapatite synthesized from sea shells through wet chemical synthesis," *Materials Letters*, vol. 97, pp. 121–124, 2013.
[14] S. Rujitanapanich, P. Kumpapan, and P. Wanjanoi, "Synthesis of hydroxyapatite from oyster shell via precipitation," *Energy Procedia*, vol. 56, no. C, pp. 112–117, 2014.
[15] Charlena, I.H. Suparto, and D.K. Putri, "Synthesis of hydroxyapatite from rice fields snail shell (Bellamya javanica) through wet method and pore modification using chitosan," *Procedia Chemistry*, vol. 17, pp. 27-35, 2015.
[16] M.K. Alam, M.S. Hossain, M. Kawsar, N.M. Bahadur, and S. Ahmed, "Synthesis of nano-hydroxyapatite using emulsion, pyrolysis, combustion, and sonochemical methods and biogenic sources: a review," *RSC Advances*, vol. 14, no. 5. Royal Society of Chemistry, pp. 3548–3559, Jan. 22, 2024.
[17] H.B. Basri, N. Bano, S.S.B. Jikan, S. Adzila, and D.M. Zago, "Crystallographic and morphological studies of nanocrystalline hydroxyapatite synthesized from bovine bone at different calcination temperatures," *Journal of Mechanics of Continua and Mathematical Sciences*, no. 4, pp. 11–19, Nov. 2019.
[18] A. Aissa and M. Othmani, "Heavy metals removal using nano-hydroxyapatite extracted from cattle bones," *ChemistrySelect*, vol. 8, no. 13, Apr. 2023.
[19] X. Song, F. Zhou, H. Ma, Y. Liu, and G. Wu, "Defect-induced synthesis of highly dispersed hydroxyapatite-supported vanadium oxide for the oxidative dehydrogenation of cyclohexane," *ChemCatChem*, vol. 15, no. 20, Oct. 2023.
[20] A.S. Hammood, S.S. Hassan, and M.T. Alkhafagy, "Access to optimal calcination temperature for nanoparticles synthesis from hydroxyapatite bovine femur Bone Wate," *Nano Biomedicine and Engineering*, vol. 9, no. 3, pp. 228–235, 2017.
[21] O.G. Agbabiaka, I.O. Oladele, A.D. Akinwekomi, A.A. Adediran, A.O. Balogun, O. G. Olasunkanm et al., "Effect of calcination temperature on hydroxyapatite developed from waste poultry eggshell," *Scientific African*, vol. 8, Jul. 2020.

[22] D.D. Pramono and P. Puspitasari, "Comparison of physicochemical properties of hydroxyapatite from scallop shell synthesized by wet chemical method with and without sonication process," in *Proceedings of the International Conference on Green Engineering & Technology 2022 (IConGETech 2022)*, Arau: AIP Conference Proceedings, Nov. 2024, p. 040034.

[23] K.C.V. Kumar, T. J. Subha, K.G. Ahila, B. Ravindran, S.W. Chang, A.H. Mahmoud et al., "Spectral characterization of hydroxyapatite extracted from Black Sumatra and Fighting cock bone samples: A comparative analysis," *Saudi Journal of Biological Sciences*, vol. 28, no. 1, pp. 840–846, Jan. 2021.

[24] G.S. Kumar, E.K. Girija, M. Venkatesh, G. Karunakaran, E. Kolesnikov, and D. Kuznetsov, "One step method to synthesize flower-like hydroxyapatite architecture using mussel shell bio-waste as a calcium source," *Ceramics International*, vol. 43, no. 3, pp. 3457–3461, Feb. 2017.

[25] C. Ruiz-Aguilar, U. Olivares-Pinto, E.A. Aguilar-Reyes, R. López-Juárez, and I. Alfonso, "Characterization of β-tricalcium phosphate powders synthesized by sol-gel and mechanosynthesis," *Boletin de la Sociedad Espanola de Ceramica y Vidrio*, vol. 57, no. 5, pp. 213–220, Sep. 2018.

[26] M.Z.A. Khiri, K.A. Matori, M.H.M. Zaid, C.A.C. Abdullah, N. Zainuddin, I.M. Alibe et al., "Crystallization behavior of low-cost biphasic hydroxyapatite/β-tricalcium phosphate ceramic at high sintering temperatures derived from high potential calcium waste sources," *Results in Physics*, vol. 12, pp. 638–644, Mar. 2019.

[27] S. W. Lee, Y. Kim, H. T. Rho, and S. il Kim, "Microhardness and microstructural properties of a mixture of hydroxyapatite and β-tricalcium phosphate," *Journal of Asian Ceramic Societies*, vol. 11, no. 1, pp. 11–17, 2023.

[28] T.A.G. Pelizaro, A.G. Tolaba, J.E. Rodriguez-Chanfrau, Y. Veranes-Pantoja, and A.C. Guastaldi, "Influence of the application of ultrasound during the synthesis of calcium phosphates," *Journal of Bionanoscience*, vol. 12, no. 5, pp. 733–738, 2018.

[29] P.M. Derlet, "Sintering Theory," *Solutions*. Paul Scherer Institute, 2017.

[30] S.L. Kang, *Sintering: Densification, Grain Growth and Microstructure*, 1st ed. British: Elsevier, 2005.

[31] A.H. Shah and M.A. Rather, "Effect of calcination temperature on the crystallite size, particle size and zeta potential of TiO_2 nanoparticles synthesized via polyol-mediated method," *Materials Today Proceeding*, vol. 44, pp. 482–488, 2021.

[32] U. Ulusoy, "A Review of particle shape effects on material properties for various engineering applications: From macro to nanoscale," *Minerals*, vol. 13, no. 1, pp. 1–81, Jan. 01, 2023.

[33] W.Y. Jang, J.C. Pyun, and J.H. Chang, "Comparative in vitro dissolution assessment of calcined and uncalcined hydroxyapatite using differences in bioresorbability and biomineralization," *International Journal of Molecular Sciences*, vol. 25, no. 1, pp. 1–17, 2024.

[34] P. Puspitasari, A.F. Fauzi, H. Susanto, A.A. Permanasari, R.W. Gayatri, J.A. Razak et al., " Phase identification and morphology of $CaCO_3$ /CaO from Achatina fulica snail shell as the base material for hydroxyapatite," *IOP Conference Series: Materials Science and Engineering*, vol. 1034, no. 1, p. 012128, Feb. 2021.

[35] D.W. Callister, *Materials Science and Engineering An Introduction*. USA: John Willey and Sons, Inc., 2007.

[36] S.H. Jaafar, M.H.M. Zaid, K.A. Matori, S.H.A. Aziz, H.M. Kamari, S. Honda et al., "Influence of calcination temperature on crystal growth and optical characteristics of

Eu3+ Doped ZnO/Zn_2SiO_4 composites fabricated via simple thermal treatment method," *Crystals (Basel)*, vol. 11, no. 2, p. 115, Jan. 2021.

[37] H. Peng, J. Wang, S. Lv, J. Wen, and J. F. Chen, "Synthesis and characterization of hydroxyapatite nanoparticles prepared by a high-gravity precipitation method," *Ceramics International*, vol. 41, no. 10, pp. 14340–14349, 2015.

[38] P.A. Forero-Sossa, J.D. Salazar-Martínez, A.L. Giraldo-Betancur, B. Segura-Giraldo, and E. Restrepo-Parra, "Temperature effect in physicochemical and bioactive behavior of biogenic hydroxyapatite obtained from porcine bones," *Scientific Reports*, vol. 11, no. 11069, pp. 1–9 2021.

[39] B. Li, B. Guo, H. Fan, and X. Zhang, "Preparation of nano-hydroxyapatite particles with different morphology and their response to highly malignant melanoma cells in vitro," *Applied Surface Science*, vol. 255, no. 2, pp. 357–360, 2008.

[40] H.F.N. Zhorifah, P. Puspitasari, Andoko, D.I. Tsamroh, and A.A. Permanasari, "Optimization of the mastication strength of hydroxyapatite as an eggshell-based tooth filler," *AIP Conference Proceeding*, vol. 2120, no. July, 2019.

[41] M. Jevtic, M. Mitric, S. Skapin, B. Jancar, N. Ignjatovic, and D. Uskokovic, "Crystal structure of hydroxyapatite nanorods synthesized sonochemical homogeneous precipitation," *Crystal Growth & Design*, vol. 8, no. 7, pp. 2217–2222, 2008.

[42] X. Guo, H. Yan, S. Zhao, Z. Li, Y. Li, and X. Liang, "Effect of calcining temperature on particle size of hydroxyapatite synthesized by solid-state reaction at room temperature," *Advanced Powder Technology*, vol. 24, no. 6, pp. 1034–1038, Nov. 2013.

[43] G.S. Kumar, L. Sathish, R. Govindan, and E.K. Girija, "Advances utilization of snail shells to synthesise hydroxyapatite nanorods for orthopedic applications †," *RSC Advance*, vol. 5, pp. 39544–39548, 2015.

[44] E.A. Ofudje, J.A. Akande, E.F. Sodiya, G.O. Ajayi, A.J. Ademoyegun, A.G. Al-Sehemi et al., "Bioactivity properties of hydroxyapatite/clay nanocomposites," *Scientific Reports*, vol. 13, no. 1, pp. 1–12 2023.

[45] A. Kurzyk, A. Szwed-Georgiou, J. Pagacz, A. Antosik, P. Tymowicz-Grzyb, A. Gerle et al., "Calcination and ion substitution improve physicochemical and biological properties of nanohydroxyapatite for bone tissue engineering applications," *Scientific Reports*, vol. 13, no. 1, Dec. 2023.

[46] K.C.V. Kumar, T.J. Subha, K.G. Ahila, B. Ravindran, S.W. Chang, A.H. Mahmoud et al., "Spectral characterization of hydroxyapatite extracted from Black Sumatra and Fighting cock bone samples: A comparative analysis," *Saudi Journal of Biological Sciences*, vol. 28, no. 1, pp. 840–846, Jan. 2021.

[47] D. Xidaki, P. Agrafioti, D. Diomatari, A. Kaminari, E. Tsalavoutas-Psarras, P. Alexiou et al., "Synthesis of hydroxyapatite, β-Tricalcium phosphate and biphasic calcium phosphate particles to act as local delivery carriers of curcumin: Loading, release and in vitro studies," *Materials*, vol. 11, no. 4, pp. 1–13, 2018.